Roles of the Disulfide Bond and Adjacent Residues in Determining the Reduction Potentials and Stabilities of Respiratory-Type Rieske Clusters†

Ellen J. Leggate and Judy Hirst*

Medical Research Council Dunn Human Nutrition Unit, Wellcome Trust/MRC Building, Hills Road, Cambridge, CB2 2XY, U.K.

Received February 1, 2005; Revised Manuscript Received March 14, 2005

ABSTRACT: Rieske [2Fe-2S] clusters have reduction potentials which vary by over 500 mV, and which are pH dependent. In the cytochrome bc_1 complex, the high-potential and low-pK values of the cluster may be important in the mechanism of quinol oxidation. Hydrogen bonds, from both side-chain and mainchain groups, are crucial for these properties, but solvent accessibility and a disulfide bond (present in only high-potential Rieske proteins) have been suggested to be important determinants also. Previous studies have addressed the hydrogen bonds, disulfide bond, and a leucine residue which may restrict solvent access, by mutations in the cytochrome bc_1 complex. However, influences on the complex (disruption of quinol binding and displacement of the Rieske domain) are difficult to deconvolute from intrinsic effects on the Rieske cluster. Here, the effects of similar mutations on cluster potential, pK values, and stability are characterized comprehensively in the isolated Rieske domain of the bovine protein. Hydrogen bonds from Ser163 and Tyr165 are important in increasing the reduction potential and decreasing the pK values. The disulfide has a limited effect on the redox properties, but is crucial for cluster stability, particularly in the oxidized state. Mutations of Leu142 had little effect on cluster potential, pK values, or stability, in contrast to the significant effects which were observed in the complex. The sum of the effects of all the mutated residues accounts for most of the differences between high- and low-potential Rieske proteins.

Rieske clusters are [2Fe-2S] clusters in which one of the iron centers is coordinated by two histidines instead of by two cysteines (*1*−*3*). The histidine ligands exert a significant effect on the cluster properties. They are neutral and electron withdrawing, so in the reduced ($[2Fe\text{-}2S]^{1+}$) state the extra electron is localized on the histidine ligated iron, and the reduction potentials of Rieske clusters are generally higher than those of all-cysteine ligated clusters (*3, 4*). In addition, they can ligate the cluster either as neutral imidazole or as negative imidazolate (*5*). Imidazolate is less effective in stabilizing extra negative charge in the reduced state, and so, at high pH, Rieske clusters have lower reduction potentials, comparable to those of all-cysteine ligated [2Fe-2S] clusters (*4*). Consequently, and because the imidazole ligands deprotonate more easily when the cluster is oxidized, Rieske cluster reduction potentials are pH-dependent (*4, 6, 7*). Although it is now known that all Rieske clusters exhibit pH-dependent reduction potentials, their cluster potentials and histidine pK values vary significantly (*3, 8*). High-potential Rieske proteins, which are essential components of the respiratory cytochrome bc_1 and photosynthetic cytochrome b_6f complexes (*9*), typically have reduction potentials of +0.35 to +0.15 V at pH 7. Low-potential Rieske-type ferredoxins (such as BphF[1], from *Burkholderia* sp. strain LB400), involved in the bacterial catabolism of aromatic compounds, have lower reduction potentials, typically −0.15 V (*10, 11*). Furthermore, the potentials of the high-potential proteins are pH-dependent above pH ∼7, but those of the low-potential proteins remain pH independent up to pH ∼10, because the pK values of their histidine ligands are higher (*8*). Significant effort has been put into understanding how the potentials and pK values of Rieske clusters are determined, both in the isolated protein (*3, 8*) and in the complex (*12, 13*), and into determining their importance in oxidation (and perhaps deprotonation) of quinol at the Q_O site of the cytochrome bc_1 and b_6f complexes (*14*−*18*).

The overall structures of the cluster-binding domains of high- and low-potential Rieske proteins are very similar (*2, 10, 19*−*22*). The high-potential proteins are distinguished by extra hydrogen bonds to the cluster and by a disulfide bond between the two cluster-coordinating loops. Site-directed mutations in the cytochrome bc_1 complex suggested that both are important in elevating the cluster potential; the mutations also exerted significant effects on the activity of the complex (see below). However, in most cases, potentials were reported at only one pH value, neglecting the influence of the histidine pK values on potential and activity, and cluster stabilities were not considered an additional possible influence on apparent activity. Furthermore, when evaluated

† This work was supported by The Medical Research Council.

* To whom correspondence should be addressed: Medical Research Council Dunn Human Nutrition Unit, Wellcome Trust/MRC Building, Hills Road, Cambridge, CB2 2XY, U.K. Phone, +44 1223 252810; fax, +44 1223 252815; e-mail, jh@mrc-dunn.cam.ac.uk.

[1] Abbreviations: BphF, low potential Rieske ferredoxin from *Burkholderia* sp. strain LB400; *Bt*Rp, overexpressed soluble domain of the bovine Rieske protein; NEM, *N*-ethylmaleimide; PFV, protein film voltammetry; PGE, pyrolytic graphite edge; $pK_{ox1,2}$, average of pK_{ox1} and pK_{ox2}; $pK_{red1,2}$, average of pK_{red1} and pK_{red2}; TCEP, tris[2-carboxyethylphosphine]hydrochloride.

10.1021/bi050189x CCC: $30.25
Published on Web 04/16/2005

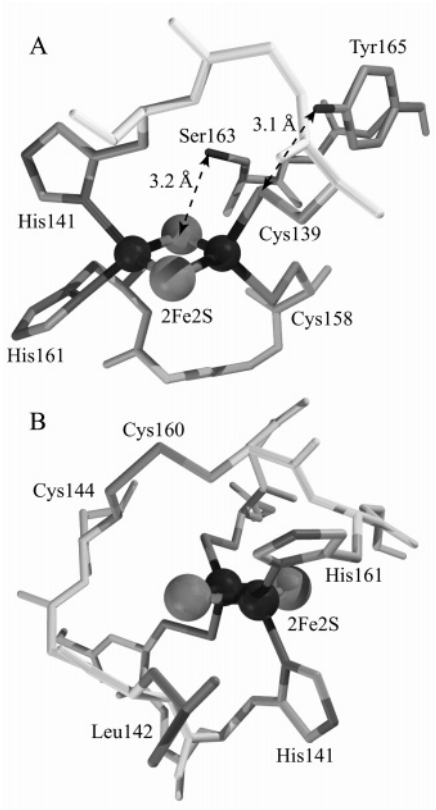

FIGURE 1: Structures of *Bt*Rp (*2*) in the vicinity of the Rieske cluster: (A) hydrogen-bonding interactions from Ser 163 and Tyr 165; (B) the position of Leu142 and the disulfide bond, both of which are surface exposed, and which help to obscure the cluster from solvent. L142 Cδ1 is 3.6 Å from Cϵ1 of H161 and 3.7 Å from Cϵ1 of H141.

in the cytochrome bc_1 complex, Rieske-protein mutants provide convoluted information: it is difficult to distinguish effects on the cluster from effects on the complex (for example, position of the Rieske headgroup or integrity of the Q_O site).

Here, the potentials, p*K* values, and cluster stabilities of three classes of high-potential Rieske protein mutants are defined, using the structurally characterized soluble domain of the Rieske protein from the bovine cytochrome bc_1 complex (*2*), overexpressed in *Escherichia coli*. Each class embodies a clear difference between high- and low-potential Rieske proteins, and the results provide a comprehensive picture of how the potentials, p*K* values, and cluster stabilities are determined. Comparison with the results of equivalent mutations in the cytochrome bc_1 complex provides insight into the effects of the Rieske cluster potential, p*K* values, and stability on catalysis.

Hydrogen Bonds to the Cluster. In the high-potential Rieske protein from the bovine cytochrome bc_1 complex there are seven hydrogen bonds to the cluster, five NH → S interactions from the protein backbone, and two OH → S interactions, from Ser163 Oη to cluster S1, and from Tyr165 Oη to Cys139 Sγ (a ligand) (Figure 1A) (*2*). They increase the cluster potential by delocalizing negative charge density, preferentially stabilizing the reduced state. The two OH → S interactions have been studied previously, by mutations in the cytochrome bc_1 complexes of *Saccharomyces cerevisae* (*23*), *Paracoccus denitrificans* (*24*), and *Rhodobacter sphaeroides* (*25*). Significant decreases in potential were observed (from 130 mV (pH 7.0) for *S. cerevisae* S183A to 44 mV (pH 6.0) for *P. denitrificans* Y159F), and the catalytic rate was suggested to depend exponentially on cluster potential (*23*). In *R. sphaeroides*, the decreased catalytic activities of the Y156H, -L, -F, and -W mutants were proposed to be due to the increased p*K* value of Y156W ($\Delta pK = +1$) as well as to the decreases in reduction potential observed (from only 4 mV in Y156H to 114 mV in Y165W) (*25*). The high-potential Rieske protein of *Thermus thermophilus*, which naturally contains Ala in place of Ser (*4*, *22*), and the low-potential Rieske proteins, which lack five of the hydrogen bonds to the bovine cluster (*8*, *10*), provide further support for the influence of S163 and Y165. Here, we describe the potentials, p*K* values, and stabilities of the S163A, Y165F, and Y165W mutants of the bovine Rieske protein.

The Disulfide Bond. High-potential Rieske clusters, such as *Bt*Rp, are ligated by the conserved motif *Cys*-X-*His*-X-Gly-Cys*-X_{12-44}-*Cys*-X-Cys*-*His* (cluster ligands are in italics; the asterisked residues form a disulfide bond which bridges over the cluster, connecting the two cluster-binding loops (Figure 1B) (*2*)). The importance of the disulfide was indicated first by specific destruction of the Rieske cluster, in mitochondria, by 2,3-dimercaptopropanol, a disulfide reductant (*26*). Later, mutations of one of the two disulfide-cysteines in the cytochrome bc_1 complexes of *R. capsulatus* (*27*) and *R. sphaeroides* (*28*) resulted typically in the complete lack of any cluster, precluding investigation of the influence of the disulfide on the cluster: only the *R. capsulatus* C155S mutant contained a low amount (<5%). Recently, among a range of double mutants in the cytochrome bc_1 complex of *S. cerevisae*, the Tyr−Leu (YL) and Tyr−Val (YV) variants contained close to stoichiometric amounts of Rieske protein and observable amounts of cluster (*29*). Only negligible catalytic activities were observed, probably because the mutants have decreased reduction potentials (~ 105 mV) and disrupted quinol binding sites (they did not respond to stigmatellin), as well substoichiometric cluster levels. Interestingly, cluster stability appeared to be uncompromised.

Previously, we described chemical reduction and reformation of the disulfide in the thermostable Rieske domain of the cytochrome bc_1 complex from *T. thermophilus* (*30*). However, the behavior we observed was complex. The cluster potential decreases upon disulfide reduction, but much of the decrease is due to the proximity of the negatively charged thiolates; measurements at low pH (to protonate them) resulted in spontaneous reformation of the disulfide upon cluster oxidation. Mutations of the two cysteine residues should avoid these complications, and two such classes of mutant are described here. The single mutants, CA and CS, mimic the sulfhydryl state and are compared to the *R. capsulatus* C155S mutant (*27*). The AA, AL, VL, and WL double mutants are based on the sequences of the low-potential Rieske-type proteins, in which the disulfide is replaced by a pair of hydrophobic residues in van der Waals contact (*10*); they complement recent studies in the cytochrome bc_1 complex of *S. cerevisae* (*29*). For each mutant, the cluster reduction potentials, p*K* values, and cluster stabilities, are described in detail, leading to a new proposal for the role of the disulfide bond in high-potential Rieske proteins.

Leucine 142. L142 is conserved in high-potential Rieske proteins, in the first half of the cluster-binding motif (*Cys*-Thr-*His*-Leu-Gly-Cys*). Typically, a Gly residue replaces Leu in low-potential Rieske-type proteins (*10*). The L136G, -D, -H, and -R mutants of the *R. capsulatus* cytochrome bc_1 complex contained substoichiometric amounts of Rieske protein and exhibited negligible activities (*31*). Their Rieske clusters had perturbed EPR spectra and decreased potentials (L136D, 75 mV; L136R, 32 mV; L136H, 21 mV; L136G, 14 mV (pH 7)), and they were unable to sense the Q-pool redox state or bind stigmatellin properly, indicating severe impairment of the Q_O site. The L136A and L136Y mutants possessed higher activity (~25%), although their potentials were also decreased (45 mV, pH 7) (*32*). Most probably, the hydrophobic Ala and Tyr residues resemble L142 more closely within the structure of the Q_O site. Thus, in mutants of L142 in the cytochrome bc_1 complex, effects on the cluster are convoluted with alterations of the Q_O site. Here, L142 mutants aimed to test the proposal that the hydrophobic Leu side chain occludes the cluster from solvent, promoting the "coupling" of cluster reduction and histidine protonation and raising the potential (*8*). In addition, because the Leu side chain is close to the side chains of the two histidine ligands (Figure 1B), we aimed to use mutations of L142 to introduce point charges close to the histidine ligands, to modify their p*K* values as well as the cluster reduction potential. Recently, a combined density functional theory/continuum electrostatics approach has suggested that extra negatively charged, surface-exposed residues in the low-potential Rieske ferredoxin, BphF, are important for its low-reduction potentials and high-p*K* values (*33*), and the L142D and K mutants form an experimental test for this proposal.

EXPERIMENTAL PROCEDURES

Cloning, Expression, and Purification of BtRp. Design of the recombinant, truncated bovine Rieske protein (*Bt*Rp) was based on the structures of the Rieske protein in the cytochrome bc_1 complex (*34*) and the soluble Rieske cluster-binding domain, resolved from the bovine cytochrome bc_1 complex by proteolysis (*2*). The soluble domain lacks the N-terminal membrane-spanning α-helix, but otherwise retains native structure and properties (*3, 35, 36*). In *Bt*Rp, the first residue was Ala70, and a six-histidine tag was introduced to the N-terminus, to give Met-Ser-$(His)_6$-Ala^{70}-Met^{71}-Ser^{72}. PCR was used to amplify the required section of DNA from a bovine heart cDNA library, using expand DNA polymerase (Roche Diagnostics Gmbh) and the following primers: forward, TAGGAATTCTC.**ATG**.AGC.*CAT.CAT.CAC.CAT.CAT.CAC*.GCC.ATG.TCG.AAA.ATT.GAA.ATC.AAG (*Bsp*HI restriction site underlined, initiator methionine codon in bold, six-histidine codons in italics); reverse, CAGAAGCTT.**CTA**.ACC.AAC.AAT.CAC.CAT.ATC.ATC.GCT. GG (*Hin*dIII restriction site underlined, stop codon in bold). Following digestion with *Bsp*HI and *Hin*dIII (New England Biolabs Inc.), the insert was ligated into the complementary *Nco*I and *Hin*dIII sites of the pIC expression vector (a derivative of pET11a provided by Dr. E. R. S. Kunji, Dunn Human Nutrition Unit) and checked by direct sequencing of both strands.

A single colony of *E. coli* strain C41(DE3) was transformed and grown overnight (37 °C, TYE−agar plate containing 100 μg mL^{-1} ampicillin (Melford Laboratories Ltd.)). A 5 mL aliquot of 2 × TY medium (containing 100 μg mL^{-1} ampicillin) was inoculated and incubated overnight at 37 °C, and then 0.5 mL aliquots were used to inoculate 500 mL volumes of the same ampicillin-containing medium (with 100 μM L-cysteine and 100 μg mL^{-1} ferric ammonium citrate (Sigma-Aldrich Ltd.)). Cells were grown aerobically at 25 °C until OD_{600} ~0.1, then induced by 100 μM isopropyl β-D-thiogalactopyranoside (IPTG, Melford Laboratories Ltd.). Following overnight growth at 25 °C, the cells were harvested by centrifugation, resuspended in a minimal volume of 50 mM Hepes (pH 8.0) containing 0.3 M NaCl and one complete EDTA-free protease inhibitor cocktail tablet per 25 mL (Roche Diagnostics Ltd.), and stored at −20 °C. This protocol maximized cluster incorporation (rather than protein yield) and minimized inclusion body formation.

Purification of *Bt*Rp was carried out at 4 °C. Cells were thawed on ice, lysed by double passage through a French press (16 000 psi), and centrifuged (200 000*g* for 30 min). The supernatant was filtered, then loaded onto a preequilibrated (buffer A: 50 mM Hepes and 0.3 M NaCl, pH 8.0) column of Ni−NTA superose (Qiagen, 1 mL per liter of cell culture). The column was washed with 8 vol of buffer A, then with buffer A containing 40 mM imidazole. *Bt*Rp was eluted with buffer A containing 250 mM imidazole, dialyzed back into buffer A, and concentrated using a YM10 membrane (Millipore Corp.). Preparations yielded up to 6 mg of highly pure *Bt*Rp per liter of culture. Gel filtration chromatography (Sephacryl S-100, Amersham Biosciences, 50 mM Hepes and 0.2 M NaCl, pH 8.0) demonstrated that *Bt*Rp was monomeric and monodisperse. Purified *Bt*Rp was stable at 4 °C for at least a week; it could also be frozen in 50% glycerol. The molecular mass of *Bt*Rp was confirmed by electrospray mass spectrometry in the positive ion mode (Sciex API III$^+$ spectrometer) following reverse-phase HPLC with an acetonitrile gradient (0.1% TFA, Perkin-Elmer Aquapore RP-300 column). The observed mass (15 112.4 Da, SD = 0.8), was close to the expected mass (15 114.3 Da); the 2 Da decrease is attributable to the formation of an additional disulfide upon denaturation. For determination of iron/protein ratios, protein concentrations were measured using the Pierce bicinchoninic acid (BCA) method, and iron concentrations were measured using the bathophenanthroline method of Doeg and Ziegler (*37*).

Site-Directed Mutagenesis and Preparation of BtRp Mutants. The primers used to create point mutations in the *Bt*Rp expression plasmid are summarized in Table S1 (Supporting Information). Mutants were cloned using a modification of the Stratagene QuikChange site-directed mutagenesis kit. The expression plasmid was amplified by PCR, using *PfuTurbo* DNA polymerase (Stratagene), in the presence of the mutagenesis primers, then the unmodified plasmid was selectively digested with *Dpn*I (New England Biolabs Inc.). The mutagenized plasmids were amplified by transformation into *E. coli* strain XL1-Blue and confirmed by direct sequencing of both strands. Plasmids for the overexpression of double mutants of *Bt*Rp were created by sequential single mutations.

Unless otherwise stated, mutants of *Bt*Rp were overexpressed and purified by the protocols described above. In some cases, lower iron-to-protein ratios were observed. Therefore, all mutants of *Bt*Rp were coexpressed with the

isc gene cluster (*38*) (plasmid supplied by Prof. Y. Takahashi, Osaka University, all growth media supplemented by 10 μg mL^{-1} tetracycline), and this significantly increased the lower values. Some of the *Bt*Rp mutants were oxygen sensitive, and so all mutants were purified in a room-temperature glovebox (O_2 < 2 ppm; Belle Technology, U.K.). For mutants obtained in lower yields, column bed volumes of 0.5 mL per liter culture were employed, and the buffer for the second wash step contained only 20 mM imidazole. Gel filtration chromatography was used routinely for purification of the mutants and demonstrated that they were monomeric and monodisperse. The exception was Y165W which eluted in two distinct peaks: this mutant is generally unstable and may be partially misfolded or degraded. The molecular mass of each mutant was confirmed by mass spectrometry; all values were within 2 Da of the expected values. The VL, WL, and Y165W mutants typically contained only 1.6 irons per protein, and L142D, despite being obtained in high yield and high purity, contained only 0.7 irons per protein; all other mutants contained close to stoichiometric amounts. The CA and CS mutants had to be purified as quickly as possible, since they tend to precipitate, even when kept strictly anaerobic.

Disulfide Reduction and Sulfhydryl Alkylation. The disulfide bond in *Bt*Rp was reduced by incubation of *Bt*Rp (200 μM, pH 8.0) with a 20-fold excess of tris[2-carboxyethylphosphine]hydrochloride (TCEP, Perbio Science U.K. Ltd.) for 2 h, at room temperature, under anaerobic conditions. Free sulfhydryl groups were alkylated by reaction with a 20-fold excess of *N*-ethylmaleimide (NEM) for 30 min, at room temperature, under anaerobic conditions. The stoichiometries of the alkylation reactions were confirmed by mass spectrometry (*30*).

UV−Visible and EPR Spectroscopies. UV−visible spectra were recorded using anaerobically sealed quartz cuvettes and a UV-1601 Shimadzu spectrometer. Samples for electron paramagnetic resonance (EPR) spectroscopy (100−150 μM) were either frozen as prepared or treated with a 5-fold excess of sodium hydrosulfite (dithionite) or L-ascorbic acid, under anaerobic conditions. Spectra were recorded on a Bruker EMX X-band spectrometer using an ER 4119HS high-sensitivity cavity, maintained at low temperature by a ESR900 continuous-flow liquid helium cryostat (Oxford Instruments, U.K.); the sample temperature (10 K) was measured by a calibrated Cernox resistor (Lake Shore Cryotronics Inc., OH). The following conditions were applied: microwave frequency ~9.38 GHz, modulation amplitude 10 G, modulation frequency 100 kHz, time constant 10.24 ms, and conversion time 40.96 ms. The microwave power, 50 μW, was low enough so that no signal distortions due to saturation were observed. Spectra were modeled using the Bruker Win-EPR SimFonia program and a Lorentzian line shape; values of $\theta = 400$ and $\phi = 40$ were used to ensure convergence. Spin quantification was carried out using EPR spectroscopy, by comparison of the spectrum of the Rieske cluster with that of a 1 mM $CuSO_4$ standard. The spectra were recorded under identical (nonsaturating) conditions in standardized EPR sample tubes. The ratio of spin concentrations was calculated from the ratio of the double integrals divided by g_{av}.

Protein-Film Voltammetry. Reduction potentials were measured using protein-film voltammetry as described previously (*30*, *39*). Briefly, the protein was applied directly to a pyrolytic graphite edge electrode surface, freshly polished with 1 μm alumina (Buehler, IL), and then placed into solution in an all-glass cell. The cell was thermostated at 20 °C and encased in a Faraday cage and an anaerobic glovebox (O_2 < 2 ppm, Belle Technology, U.K.). The reference electrode was a standard calomel electrode; all potentials are reported relative to the standard hydrogen electrode. Analogue-scan cyclic voltammetry was performed using an Autolab electrochemical analyzer (Eco-chemie, The Netherlands). Data were analyzed using Fourier transformation and an in-house analysis program (courtesy of Dr. H. A. Heering). Solution pH values were controlled using mixtures of four of the following buffers (total concentration 40 mM): 10 mM sodium acetate, Hepes, MES, TAPS, CAPS, and sodium phosphate, depending on the pH. The pH of each solution was checked immediately following measurement and, when necessary, the effects of high Na^+ concentration were corrected for. Volumetric solutions of NaOH were used at and above pH 13.

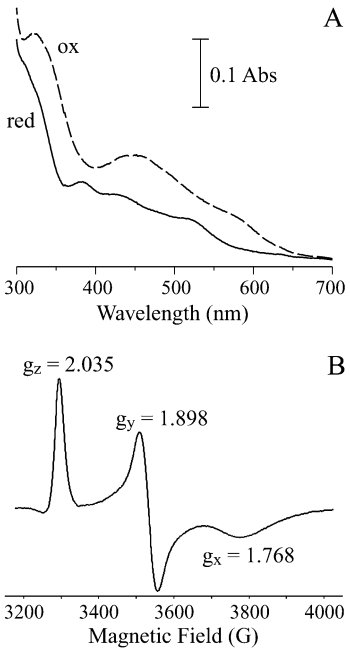

FIGURE 2: (A) UV−Visible spectra of oxidized (dashed line, maxima at 323, 458, and 579 nm) and reduced (solid line, maxima at 305, 383, 428, and 520 nm) wild-type *Bt*Rp. Protein concentration 25 μM, in 50 mM Hepes (pH 8.0) and 0.3 M NaCl. *Bt*Rp was isolated in the reduced state and oxidized by the addition of a stoichiometric amount of potassium ferricyanide. (B) The EPR spectrum of reduced "as-isolated" *Bt*Rp (~120 μM, 50 mM Hepes (pH 8.0) and 0.3 M NaCl). EPR conditions as described in Experimental Procedures.

RESULTS

Characterization of the Overexpressed Wild-Type BtRp Rieske Cluster. Figure 2A shows the UV−visible spectra of oxidized and reduced *Bt*Rp, and Figure 2B shows the EPR spectrum of reduced *Bt*Rp (as expected oxidized *Bt*Rp was EPR silent). They demonstrate that *Bt*Rp contains a correctly formed Rieske cluster and are very similar to spectra reported for the soluble Rieske protein domain isolated from the cytochrome bc_1 complex (*3*, *35*, *36*). Spin and iron quantifications showed that all the iron was cluster-bound and that

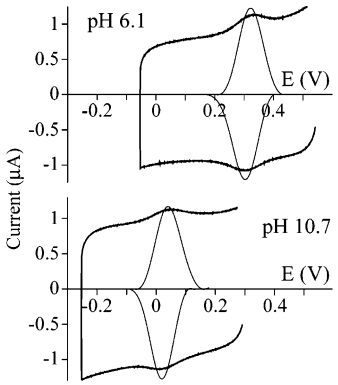

FIGURE 3: Typical protein-film voltammograms of wild-type *Bt*Rp. The raw data are displayed alongside background-subtracted signals, which are adjusted in magnitude so that a theoretically shaped (Nernstian) peak would have an amplitude equal to the *y*-axis span. All voltammograms were recorded at 0.1 V s^{-1}, 20 °C, 2 M NaCl, as described in Experimental Procedures. The potential was poised at the oxidative limit for 15 s prior to scanning.

>90% of the *Bt*Rp molecules contained correctly incorporated clusters.

Reduction potentials for *Bt*Rp were measured over a wide range of pH, using protein-film voltammetry (PFV). As described previously, reduction potentials were measured in 2 M NaCl to minimize the influence of charge reversal at the isopotential point and to allow all measurements to be made at the same ionic strength, even at very alkaline pH values (*4*, *8*, *39*). Typical voltammograms are presented in Figure 3. The oxidation and reduction peaks are both clearly defined, and their maximum areas are consistent with a protein (sub)monolayer. The peak shapes and separations are close to their ideal Nernstian values, and the average peak position, the reduction potential, did not change as the scan rate was decreased. Therefore, adsorbed *Bt*Rp is thermodynamically homogeneous, and, on this experimental time scale, it exchanges electrons rapidly and reversibly with the electrode. Reduction potentials measured by PFV correspond closely to values measured by diffusional voltammetry under identical conditions, showing that the adsorbed protein retains its native conformation. In addition, they are close to values reported for the isolated Rieske protein domain (*3*, *35*): the difference is ~30 mV at pH 7.2, 25 °C, 0.01 M NaCl, either because of small differences in the experimental conditions or because of the histidine tag on *Bt*Rp.

The variation of reduction potential with pH, for wild-type *Bt*Rp, is reported in Figure 4A. As described previously in detail, the pH dependence can be modeled by using eq 1 to determine the p*K* values and reduction potentials defined by Scheme 1 (*4*). The data fit is included in Figure 4A and the parameters are reported in Table 2.

$$E_{obs} = E_{acid} - \frac{RT}{F}\ln\left[\left(1 + \frac{K_{ox1}}{a_{H^+}} + \frac{K_{ox1}K_{ox2}}{a_{H^+}^2}\right)\Big/ \left(1 + \frac{K_{red1}}{a_{H^+}} + \frac{K_{red1}K_{red2}}{a_{H^+}^2}\right)\right] \quad (1)$$

pK_{ox1} and pK_{ox2} and pK_{red1} and pK_{red2} refer to the p*K* values of the oxidized and reduced cluster, respectively, and are assigned to the two cluster-ligating histidine residues. E_{acid} is the pH-independent reduction potential of the cluster when both histidines are protonated. Figure 4B shows the corresponding Pourbaix (stability) diagram, to identify the most thermodynamically favored states at different potentials and pH values. At low pH, the histidines are fully protonated in each oxidation state; at high pH, they are fully deprotonated in each oxidation state. At intermediate pH values, the reduced state is more highly protonated than the oxidized state, and the reduction potential is pH dependent. In contrast to previous studies of other Rieske proteins by PFV, the singly protonated reduced state is observed for *Bt*Rp. Otherwise, the pH-dependent reduction potential of wild-type *Bt*Rp behaves very similarly to those of the homologous high-potential Rieske proteins from *T. thermophilus* and *R. sphaeroides*, described in detail previously (*8*).

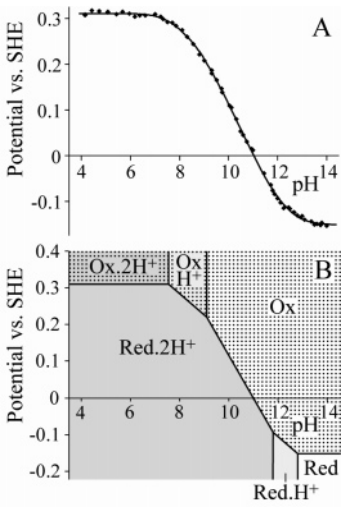

FIGURE 4: (A) Variation in the reduction potential with pH for *Bt*Rp (◆) (conditions were 0.1 V s^{-1}, 20 °C, 2 M NaCl as for Figure 3). Fits to the data (eq 1 and Scheme 1) are shown, and the parameters defined are reported in Table 2. (B) Corresponding Pourbaix (stability) diagram. Protonated states are shaded, and oxidized states are dotted.

Scheme 1: Thermodynamic Square Scheme Describing Coupled Proton and Electron Transfer to Rieske Clusters[a]

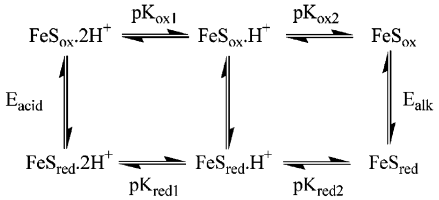

[a] E_{acid} and E_{alk} are the pH-independent reduction potentials at the acid and alkaline limits, respectively. pK_{ox1} and pK_{ox2} are the pK_a values for the two histidine ligands when the cluster is oxidized; pK_{red1} and pK_{red2} are the corresponding values for the reduced cluster.

Design of Site-Directed Mutants of BtRp. Figure 1 shows the structure of native *Bt*Rp, in the vicinity of the Rieske cluster, including the three sets of residues which were targeted. First, mutants of S163 and Y165 were designed to test the effects of removing specific hydrogen bonds (Table 1, top). Second, six variants which lack the disulfide bond were designed (Table 1, top), and the disulfide of *Bt*Rp was also modified chemically, by reduction and by reduction followed by alkylation (Table 1, bottom) (*30*). Third, mutants of L142A were designed to increase solvent access to the Rieske cluster by substitution of the hydrophobic side chain,

Table 1: Variants of *Bt*Rp Produced by Site-Directed Mutagenesis, Disulfide and Sulfhydryl Variants Produced Chemically

Mutants of *Bt*Rp

variant	disulfide	designation	rationale
S163A	√	S163A	Eliminates the hydrogen bond from the hydroxyl group of S163 to cluster S1 (*2*).
Y165F	√	Y165F	Eliminates the hydrogen bond from the hydroxyl group of Y165 to the Sγ of C139 (a cluster ligand) (*2*).
Y165W	√	Y165W	Eliminates the hydrogen bond from the hydroxyl group of Y165 to the Sγ of C139; large change in p*K* reported previously in cytochrome bc_1 complex (*25*).
C144A C160A	×	AA	Alanine side chains are neutral and relatively small—no steric interference expected.
C144A C160L	×	AL	Common motif in low-potential "Rieske-type" proteins, in place of the disulfide (*10*).
C144V C160L	×	VL	Valine is intermediate in size, between alanine and tryptophan.
C144W C160L	×	WL	Common motif in low-potential "Rieske-type" proteins, in place of the disulfide (*10*).
C160A	×	CA	(Simple, single mutations, which mimic the disulfhydryl form but cannot form the disulfide equivalent.
C160S	×	CS	May allow the influence of thiol protonation to be explored.)
L142A	√	L142A	Decreases the size of the hydrophobic side chain, which is proposed to shield the cluster from solvent (*8*).
L142D	√	L142D	Introduces a negative charge close to the cluster and the histidine ligands.
L142K	√	L142K	Introduces a positive charge close to the cluster and the histidine ligands.

*Bt*Rp variants

variant	disulfide	production
*Bt*Rp-TCEP	×	Wild-type *Bt*Rp treated with TCEP to reduce the disulfide to two sulfhydryls (*30*). These can be deprotonated (negative) or protonated (neutral).
*Bt*Rp-NEM	×	Wild-type *Bt*Rp treated with TCEP to reduce the disulfide to two sulfhydryls, and then with NEM to alkylate the sulfhydryls (*30*). Alkylated sufhydryls are uncharged.
CA-NEM	×	CA mutant treated with NEM to alkylate the single cysteine residue irreversibly. Cys-NEM is a neutral residue.
CS-NEM	×	CS mutant treated with NEM to alkylate the single cysteine residue irreversibly. Cys-NEM is a neutral residue.

Table 2: Reduction Potentials and p*K* Values for Variants of *Bt*Rp[a]

variant	pH range	E_{acid}, mV	E_{alk}, mV	pK_{ox1}	pK_{ox2}	pK_{red1}	pK_{red2}
WT	4.0−14.0	311	−152	7.55	9.10	11.80	12.81
S163A	4.5−14.0	164	−297	8.15	9.31	11.88	13.54
Y165F	3.7−14.0	252	−225	7.74	9.43	12.08	13.31
Y165W	4.7−13.0	214	< −216	8.00	9.40	> 12.40	
AA	4.4−12.6	257	< −177	7.84	9.26	> 12.20	
AL	4.7−11.0	235	< −212	7.83	9.09	> 12.30	
VL	5.4−12.7	172	< −243	8.33	9.34	> 12.40	
WL	4.7−12.8	246	< −198	7.80	9.16	> 12.30	
WT-NEM	5.0−12.8	255	< −179	7.89	9.24	> 12.30	
CA	4.2−12.3	246	< −165	7.82	9.12	> 12.00	
CA-NEM	4.5−12.6	251	< −169	7.98	9.40	> 12.30	
CS	4.5−12.0	235	< −152	8.07	9.28	> 12.00	
CS-NEM	4.5−12.3	235	< −183	8.12	9.29	> 12.30	
L142A	3.7−14.0	287	−148	7.94	9.47	11.83	13.06
L142D	4.4−12.1	284	< −80	7.97	9.79	> 12.00	
L142K	3.7−14.0	326	−149	7.22	9.31	11.53	13.18

[a] Parameters are defined by Scheme 1, and derived from the fits to the data (Figures 4 and 8). Where exact values for E_{alk}, pK_{red1}, and pK_{red2} cannot be determined, the maximum value for E_{alk} and the minimum average value for pK_{red1} and pK_{red2}, are reported. Errors are typically ±3 mV for E_{acid}, ±20 mV for E_{alk}, ±0.1 for p$K_{ox1,2}$, and ±0.2 for p$K_{red1,2}$.

and to introduce extra charges close to the histidine ligands, with the aim of modulating their p*K* values (Table 1, top).

Spectroscopic Characterization of Variants of BtRp. The twelve mutants of *Bt*Rp (Table 1, top), and the four further variants which were created by disulfide bond reduction and/or alkylation (Table 1, bottom), all showed UV−visible spectra which were typical of Rieske proteins in the reduced state (as isolated, data not shown). In each case, the spectra were very similar to that of wild-type *Bt*Rp (Figure 2A), with slight variations in the positions (≤10 nm) and widths of some of the bands. The largest differences were observed for S163A, Y165F, and Y165W, consistent with the removal of a hydrogen bond modulating the electronic structure of the cluster. The spectra confirmed that Rieske clusters were incorporated correctly into each of the mutants during expression or retained during chemical modification.

EPR spectra were recorded for each variant of *Bt*Rp and were all typical of Rieske clusters, with *g*-values altered only slightly with respect to wild-type *Bt*Rp. The shape of the g_x component was sharper than that of wild-type *Bt*Rp for the hydrogen-bond mutants (particularly S163A) and broader for the disulfide-bond double-mutants (particularly VL and WL) and for the L142 mutants. The spectra of S163A, AL, and L142A are representative examples and are presented in Figure 5. The *g*-values and line widths for every mutant are reported in Table S2 (Supporting Information). Initial EPR samples of the CA and CS mutants, prepared following gel-filtration, clearly contained multiple species. However, the spectrum included in Figure 5 shows only a typical Rieske cluster; this sample was purified as quickly as possible, under strictly anaerobic conditions, and immediately after elution from the Ni−NTA column. Further experiments confirmed that the CA and CS mutants are unstable, perhaps due to dimerization and aggregation via their free thiol groups.

For comparison of the different EPR spectra, Figure 6 shows a plot of the *g*-values for the 16 variants, against their rhombicities (R_z, eq 2). For Rieske and Rieske-type proteins,

$$R_z = \frac{300(g_y - g_x)}{((2g_z - g_y) - g_x)} \qquad (2)$$

approximately linear relationships have been established between the *g*-values and R_z (*3*), and so Figure 6 aids in classifying the behaviors of the different variants and in identifying outliers. In accordance with Figure 6, Y165W and VL are clearly distinct from the other variants; VL also has anomalous voltammetric properties (see below). It is possible that the clusters in Y165W and VL are structurally distorted, perhaps because of newly formed steric interac-

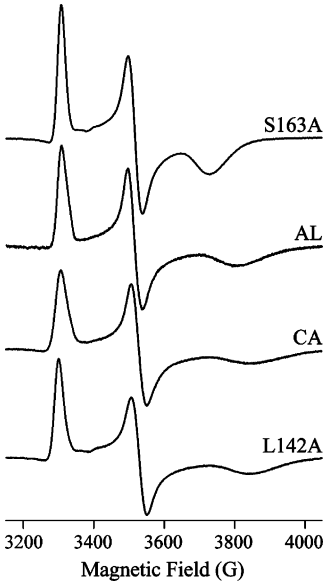

FIGURE 5: The EPR spectra of representative mutant forms of *Bt*Rp, normalized to equal spin concentrations (~120 μM, 50 mM Hepes (pH 8.0) and 0.3 M NaCl). EPR conditions as described in Experimental Procedures; *g*-values are reported in Table S2 (Supporting Information).

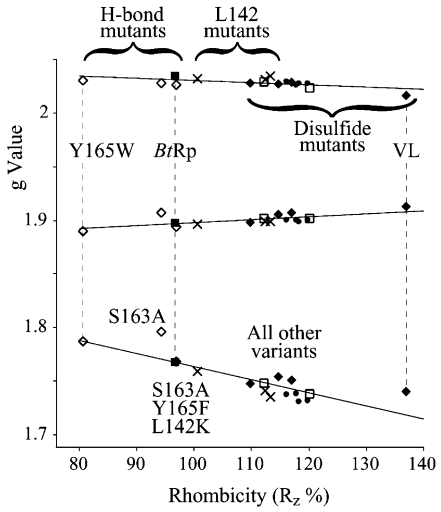

FIGURE 6: Plot of g_x, g_y, and g_z values for each mutant, derived from the EPR spectra, as a function of the rhombicity (R_z), and best-fit lines through the data. Values of R_z > 100% correspond to R_x values of approximately (200% − R_z). Different symbols are used for different classes of variants: ■, wild-type *Bt*Rp; ◇, hydrogen-bond mutants (S163A, Y165F, Y165W); ×, mutants of L142; ◆, double mutants of the two disulfide bonding cysteines; □, *Bt*Rp-TCEP and *Bt*Rp-NEM; ●, CA, CS, CA-NEM, and CS-NEM. Exact values of g_x, g_y, and g_z are given in Table S2 (Supporting Information).

tions. This observation is consistent with the heterogeneity/instability of these two mutants, suggesting that they are not good candidates for studying the isolated effects of disulfide and hydrogen bond alterations. The C164Y:C180L (YL) and C164Y:C180V (YV) mutants studied recently in the *Saccharomyces cerevisae* cytochrome bc_1 complex showed similar large increases in cluster rhombicity (*29*).

Protein-Film Voltammetry of Variants of BtRp. Figure 7 shows example voltammograms from each class of the variant forms of *Bt*Rp, recorded at pH ~8. Although the peak areas vary, in all cases the voltammetric behavior is similar to that of wild-type *Bt*Rp, with compact peaks and small

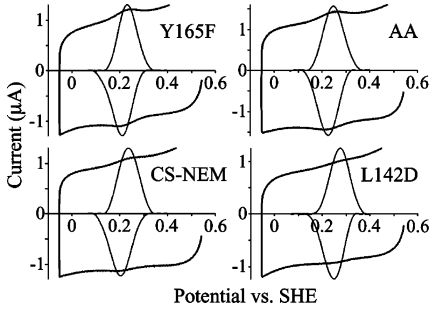

FIGURE 7: Voltammograms recorded for examples of each class of *Bt*Rp variant, presented as in Figure 3. All voltammograms were recorded at 0.1 V s^{-1}, 20 °C, 2 M NaCl, as described in Experimental Procedures. The pH values were 7.94 (Y165F), 7.94 (L142D), 7.92 (AA), and 7.96 (CS-NEM). L142D is an example of a mutant which gives poorly defined peaks, visible over only a limited range of pH.

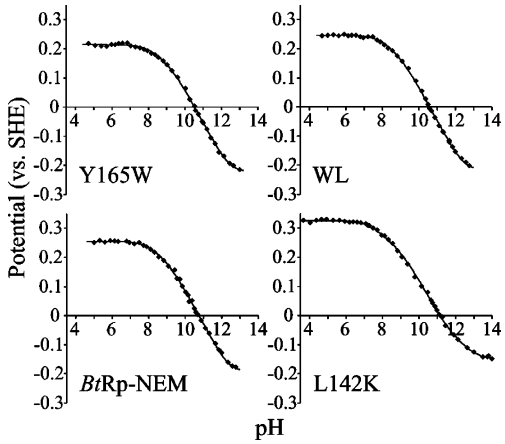

FIGURE 8: Variation in the reduction potential with pH, for four representative variants of *Bt*Rp (conditions were 0.1 V s^{-1}, 20 °C, 2 M NaCl, as described for Figure 7) and fits to the data (using eq 1 and Scheme 1). The parameters defined are reported in Table 2.

peak-to-peak separations. As may be expected from its heterogeneity, Y165W gave poorly defined peaks. The signals from L142D were also very weak, perhaps because the extra negative charge weakens the adsorption to the surface (L142K forms particularly stable films), but also because of its lower cluster content (see Experimental Procedures). The voltammetric signals from the disulfide mutants were all weaker than for wild-type *Bt*Rp, but the variants with free sulfhydryl groups (*Bt*Rp-TCEP, -CA, and -CS) showed the weakest signals of all. These variants are unstable (see above), and in reporting their potentials we rely on the assumption that any degraded clusters present do not contribute to the voltammetric signals observed. Interestingly, alkylating the free thiol groups of *Bt*Rp-TCEP, -CA, and -CS with NEM promoted the voltammetry significantly, suggesting that the negative thiols inhibit adsorption or that the alkylated proteins are more stable. Figure 8 presents the variation of potential with pH for four representative variant forms of *Bt*Rp. The parameters determined using eq 1 to fit the data are presented for all variants in Table 2.

The Effects of the Mutations on Cluster Stability. The stabilities of six representative variants of *Bt*Rp were compared: wild-type *Bt*Rp, S163A, Y165F, AA, VL, and L142K. CA and CS were not included, as their instability is most likely due to the free cysteine. The variants were

Table 3: Differences between the Reduction Potentials and p*K* Values of Variants of *Bt*Rp and Wild-Type Protein, Calculated from the Values Presented in Table 2[a]

variant	ΔE_{acid} (mV)	ΔE_{alk} (mV)	$\Delta pK_{ox1,2}$	$\Delta pK_{red1,2}$	ΔE_{acid} (kJ mol^{-1})	$\Delta pK_{ox1,2}$ (kJ mol^{-1})
S163A	−147	−145	0.41	0.41	14.2	2.3
Y165F	−59	−73	0.26	0.39	5.7	1.5
Y165W	−97		0.38		9.4	2.1
AA	−54		0.28		5.2	1.6
AL	−76		0.14		7.3	0.8
VL	−139		0.51		13.4	2.9
WL	−65		0.16		6.3	0.9
WT-NEM	−56		0.24		5.4	1.3
CA	−65		0.15		6.3	0.8
CA-NEM	−60		0.37		5.8	2.1
CS	−76		0.35		7.3	2.0
CS-NEM	−76		0.38		7.3	2.1
L142A	−24	+4	0.38	0.14	2.3	2.1
L142D	−27		0.56		2.6	3.1
L142K	+15	+3	−0.06	0.05	−1.4	−0.3

[a] Errors are typically ±3 mV for E_{acid}, ±20 mV for E_{alk}, ±0.1 for $pK_{ox1,2}$, and ±0.2 for $pK_{red1,2}$.

purified anaerobically, by affinity chromatography only; 1 mM ascorbate was added to ensure complete reduction, then the samples were dialyzed into 50 mM Hepes and 0.3 M NaCl, pH 8.0. A portion of each sample was then oxidized using a 5-fold excess of ferricyanide and redialyzed. The UV−visible spectrum of each variant, in both the oxidized and reduced states, was monitored under the following conditions: room temperature (anaerobic); room temperature + O_2 (aerobic); pH 4, room temperature (anaerobic, corrected using a known volume of 0.1 M HCl). The results are presented in Table 4.

All the variants, except VL, were fully stable in the reduced state in the absence of oxygen; mutant VL degraded only slowly over the 24 h period of the experiment. In the oxidized state, in the absence of oxygen, WT-*Bt*Rp and L142K were fully stable and S163A and Y165F degraded only slowly over 24 h. However, the oxidized clusters in AA and VL were very unstable; the oxidized cluster in AA could be observed only transiently, and the oxidized cluster in VL could not be observed at all. The behavior of all the oxidized clusters was very similar whether oxygen was present or not, suggesting that oxygen acts only as an oxidant toward the reduced clusters. Consequently, the behavior of the reduced clusters in the presence of oxygen can be explained by considering that clusters which have higher potentials, such as WT-*Bt*Rp and L142K, are not oxidized by oxygen at a significant rate, but those with lower potentials (S163A, Y165F, AA, and especially VL) are susceptible. The stability of the clusters, starting from the reduced state in oxygen, is thus a combination of the rate of oxidation and the stability of the oxidized cluster. The experiments at pH 4 confirm that reduced clusters are more stable than their oxidized counterparts and that the general order of stability is WT-*Bt*Rp, L142K > S163A, Y165F ≫ AA, VL.

DISCUSSION

Hydrogen Bonds to the Cluster from S163 and Y165. The three hydrogen-bond mutants, S163A, Y165F, and Y165W, all have decreased cluster reduction potentials and increased cluster p*K* values (Tables 2 and 3). The results are consistent with the removal of a hydrogen-bonding dipole, which preferentially stabilizes the most negatively charged state (reduced or deprotonated). As discussed previously, the effects on potential are significantly greater than those on p*K* (Table 3), because the redox active iron center is closer to the hydrogen-bonding dipole than the protonation sites are and because the histidine residues are solvent-exposed (*8*). In these mutants, $E_{acid} - E_{alk}$ and $pK_{ox1,2} - pK_{red1,2}$ are not altered significantly (the $E-$pH curves (Figures 3 and 8) require only translations to map them onto the wild-type curve) (*8*). This shows that the mutations do not affect coupling between the reduction and protonation states of the cluster. The changes in E_{acid} observed (Table 3) are consistent with values reported previously from equivalent mutations in the cytochrome bc_1 complexes of *Saccharomyces cerevisae* (*23*) and *Paracoccus denitrificans* (*24*) and confirm that the effects of mutating S163 are greater than the effects of mutating Y165. This is because S163 hydrogen-bonds directly to cluster S1, placing its dipole closer to both the reducible iron center and the histidine ligands than the dipole of Y165, which hydrogen-bonds to the Sγ of cluster ligand Cys139 (Figure 1A) (*2*). The Y165W mutation is slightly more significant than the Y165F mutation, perhaps because of the steric bulk of the Trp side chain (and reflected in the instability and heterogeneity of the Y165W protein). It has been suggested that the Trp side chain contacts S163, altering its interaction with the cluster and augmenting the effects of mutating Y165 (*25*). Interestingly, although the decreased potentials of both Y165 mutants are consistent with those reported by Guergova-Kuras and co-workers, we do not observe the significantly increased pK_{ox} values of mutant Y165W ($\Delta pK_{ox1,2} > 1$) which were reported and interpreted to support the importance of the deprotonated Rieske cluster in quinol oxidation by the cytochrome bc_1 complex (*25*). Mutations of S163 and Y165 caused only small decreases in the stability of both the oxidized and reduced clusters (Table 4), consistent with disruption of the hydrogen-bonding network around the cluster.

The Roles of the Disulfide Bond. All of the disulfide variants studied, except mutant VL, gave very similar values for E_{acid} (235−257 mV, $\Delta E_{acid} = -54$ to -76 mV) and average pK_{ox} values which were increased by 0.14 to 0.38 units (Tables 2 and 3). These values are consistent with those estimated from the chemical reduction of the disulfide bond in the Rieske protein from *T. thermophilus* ($-\Delta E_{acid} \geq 40$ mV), but interpretation of the data is less ambiguous because there are no complications from deprotonation or recombination of the free thiol residues (*30*). It is likely that the lower potentials and increased p*K* values result from removal of the polarizable sulfur groups and from the release of the disulfide tether between the two cluster coordinating loops perturbing the hydrogen-bonding network and increasing solvent accessibility to the cluster region. As discussed above, the histidine p*K* values are less affected than the reduction potential because the histidine ligands are more exposed to solvent.

In designing the disulfide mutants, we expected a trend in their behavior, following the size of the residue side chains (AA < AL < VL < WL). However, mutant VL is clearly anomalous, while AA, AL, and WL are very similar. It is possible that the steric strain, which should build up as the side chains increase in size, is relieved, in WL, by an

Table 4: Stability of the Rieske Cluster under Different Conditions, in Wild-Type *Bt*Rp and Representative Mutants[a]

	reduced	reduced + O_2	oxidized	oxidized + O_2	reduced pH 4	oxidized pH 4
wild-type *Bt*Rp	stable[a]	stable[a]	stable[a]	stable[a]	partial degradation after 1 h	immediate degradation
L142K	stable[a]	stable[a]	stable[a]	stable[a]	partial degradation after 1 h	immediate degradation
S163A	stable[a]	oxidized after ~1 h	>90% remaining after 24 h	>90% remaining after 24 h	significant degradation after 1 h	immediate degradation
Y165F	stable[a]	oxidized/degraded[b]	partial degradation after 24 h	partial degradation after 24 h	partial degradation after 1 h	immediate degradation
AA	stable[a]	partial degradation after 24 h	fully degraded in <5 min[c]		immediate degradation	
VL	partial degradation after 24 h	no cluster observable after ~1 h	oxidized cluster not observable[b]		immediate degradation	

[a] "Stable" indicates that no significant spectral changes were observed after 24 h. [b] After 24 h the spectrum indicated that the cluster was predominantly oxidized. However, the spectral features were broadened, suggesting that the sample was also slowly degrading. [c] No cluster could be observed in AA or VL following oxidation with ferricyanide and dialysis. Reaction with a stoichiometric amount of ferricyanide in the UV−vis cuvette demonstrated the formation of the oxidized cluster in mutant AA only. In this case, no cluster remained after 5 min.

alternative orientation of the Trp side chain. Consequently, VL may be the most "strained" mutant, consistent with its lower stability and anomalous EPR signal. Note that the distance between the two disulfide residues in *Bt*Rp (Cβ−Cβ) is 3.7 Å (*2*), whereas in BphF, the equivalent distance (TrpCβ−LeuCβ) is 4.5 Å (*10*). Therefore, it is very likely that steric strain will be present in the *Bt*Rp variants, particularly those with larger side chains. The YL and YV mutants in the cytochrome bc_1 complex of *S. cerevisae* showed increases in rhombicity comparable to those of the *Bt*Rp VL mutant, and similarly large decreases in potential (YL 115 mV; YV 105 mV; *Bt*Rp-VL 139 mV (*29*)). However, the potential of the C155S mutant in the cytochrome bc_1 complex of *R. capsulatus* was also more significantly decreased (180 mV) than the equivalent mutants in *Bt*Rp (*27*). Therefore, it is possible that there are extra contributions operating in the cytochrome bc_1 complex, such as alterations to the position of the Rieske headgroup with respect to the Q_O site (*12, 13*).

In the cytochrome bc_1 complex, previous studies on mutants of S163 and Y165, which are buried in the Rieske protein interior and therefore unlikely to affect the Q_O-site, established a relationship between catalytic activity and Rieske cluster reduction potential (*23*). However, the decreased reduction potentials of the *S. cerevisae* cytochrome bc_1 complex YL and YV mutants are not sufficient, within this relationship, to bring about the decreases in activity which were observed (0.04%). The EPR spectra of the *S. cerevisae* YL and YV mutants and the *R. capsulatus* C155S mutant, are not responsive to Q_O-site inhibitors, suggesting that quinol binding is disrupted (*27, 29*). However, the results presented here suggest that an important role for the disulfide is to stabilize the cluster, most crucially in the oxidized state and that, in the absence of the disulfide, the cluster will degrade. Indeed, treating submitochondrial particles with 2,3-dimercaptopropanol to reduce the disulfide does result in loss of the Rieske cluster (*26*). Note also that the *R. capsulatus* C155S mutant contained only a small amount of Rieske cluster (*27*), while no cluster quantification was reported for the *S. cerevisae* YL and YV mutants (*29*).

It is clear that oxidized high-potential Rieske clusters are less stable than their reduced counterparts, the opposite trend to that predicted by the Irving−Williams series (Fe^{3+} forms stronger complexes than Fe^{2+}). However, S^{2-} is a soft ligand and is less discriminating than an oxygen or nitrogen ligand. Consequently, the oxidized cluster is less stable because disruption of the cluster to form $[Fe(H_2O)_6]^{3+}$ is more favorable energetically than disruption of the cluster to form $[Fe(H_2O)_6]^{2+}$, and so, it is likely that the disulfide impedes cluster degradation kinetically, not thermodynamically. If this is correct, then how do low-potential Rieske proteins, which do not contain a disulfide bond, maintain their cluster stability? Although it is possible that low-potential clusters are protected, as effectively, by the two van der Waals residues that replace the disulfide, it is more likely that high-potential clusters are intrinsically more susceptible to hydrolytic breakdown. Hydrogen-bonding dipoles, which are the predominant determinant of cluster potential, act by decreasing electron density on the cluster, and this has the additional consequence of increasing its susceptibility to nucleophilic attack by solvent. A tyrosine residue was proposed to play a similar role in blocking solvent access and preventing hydrolytic breakdown in high-potential iron proteins (HiPIPs) (*40*).

Mutations of L142. The L142A mutation is electroneutral, and therefore, changes in potential and p*K* are due to alterations in the solvent accessibility of the cluster or to small changes in the conformation of the protein backbone, which affect the hydrogen bond from the amide of L142 to cluster S2 (*2*). In L142A, E_{acid} has decreased by 24 mV and $pK_{ox1,2}$ has increased by 0.38 units (Table 3). The two changes are very similar energetically (2.3 and 2.1 kJ mol^{-1}, respectively) and so are unlikely to be attributable to perturbation of the hydrogen bond (which would affect E_{acid} more than $pK_{ox1,2}$). Furthermore, changes in E_{alk} (4 mV) and $pK_{red1,2}$ (0.14 units) are smaller, consistent with increased solvent access to the cluster and a small decrease in coupling between reduction and protonation ($E_{acid} - E_{alk} = 435$ mV in L142A, 463 mV in WT; $\Delta pK = 3.7$ in L142A, 4.0 in WT) (*8*).

For the L142D and L142K mutants, an additional charge is present, closer to the histidines than to the redox-active iron center. Relative to L142A, E_{acid} is decreased by 3 mV in L142D and increased by 39 mV in L142K; $pK_{ox1,2}$ is increased by 0.18 in L142D and decreased by 0.44 in L142K. Thus, the effect of the extra negative charge in L142D is small, perhaps because the Asp side chain moves away from the histidines and because the negative charge is solvated.

The effect of the positive charge in L142K is significant, and the effects on E_{acid} (3.8 kJ mol^{-1}) and p$K_{ox1,2}$ (2.5 kJ mol^{-1}) are similar. The magnitudes of the observed changes in p$K_{ox1,2}$ are consistent with the calculated effects of solvent-exposed negatively charged residues in BphF (0.3−0.6 p*K* units) (*33*). Note that the L142K mutant is the only variant which has a higher potential and lower p*K* values than wild-type *Bt*Rp.

Similar mutants in the cytochrome bc_1 complex of *R. capsulatus* caused decreases in reduction potential of up to 114 mV (L136G), and the potentials did not follow the trend predicted from the residue charge (L136R $\Delta E_7 = -32$ mV, L136D $\Delta E_7 = -75$ mV, L136G $\Delta E_7 = -114$ mV, L136A $\Delta E_7 = -45$ mV) (*31*, *32*), so it is interesting that the L142 mutations in *Bt*Rp have, comparatively, so little effect. It is likely that, in the complex, there is an additional significant contribution to these changes in reduction potential, perhaps alteration of interactions between the Rieske protein and the Q_O site or alterations in the position of the Rieske protein headgroup. Consistent with this, these mutations also caused significant decreases in catalytic rate because their Q_O-sites are perturbed and because they cannot bind quinol in a productive conformation.

Comparison with Low-Potential Rieske-Type Proteins. The sum of the effects of the S163A, Y165F, AL (a typical disulfide variant), and L142A mutations may be expected to produce a protein with potentials and p*K* values similar to that of the low-potential Rieske-type proteins. Predicted values for E_{acid} and p$K_{ox1,2}$ are $E_{acid} = 5$ mV and p$K_{ox1,2} = 9.52$. Measured values for BphF are −135 mV and 10.65 (*8*). Therefore, 70% of the difference in E_{acid} is accounted for, but only 50% of the difference in p$K_{ox1,2}$ is accounted for. The remaining difference is attributable to additional hydrogen bonds from the protein backbone in *Bt*Rp (*2*) and to the influence of extra negatively charged residues in BphF (*33*).

ACKNOWLEDGMENT

We thank Gregory Yakovlev, for carrying out some of the experiments described, and Dr. Ian M. Fearnley, for carrying out mass spectrometry measurements.

SUPPORTING INFORMATION AVAILABLE

Table S1, primers used in site-directed mutagenesis. Table S2, EPR parameters for wild-type *Bt*Rp and all variant forms. This material is available free of charge via the Internet, at http://pubs.acs.org.

REFERENCES

1. Gurbiel, R. J., Batie, C. J., Sivaraja, M., True, A. E., Fee, J. A., Hoffman, B. M., and Ballou, D. P. (1989) Electron−nuclear double resonance spectroscopy of ^{15}N-enriched phthalate dioxygenase from *Pseudomonas cepacia* proves that two histidines are coordinated to the [2Fe-2S] Rieske-type clusters, *Biochemistry 28*, 4861−4871.
2. Iwata, S., Saynovits, M., Link, T. A., and Michel, H. (1996) Structure of a water soluble fragment of the 'Rieske' iron−sulfur protein of the bovine heart mitochondrial cytochrome bc_1 complex determined by MAD phasing at 1.5 Å resolution, *Structure 4*, 567−579.
3. Link, T. A. (1999) The structures of Rieske and Rieske-type proteins, *Adv. Inorg. Chem. 47*, 83−157.
4. Zu, Y., Fee, J. A., and Hirst, J. (2001) Complete thermodynamic characterization of reduction and protonation of the bc_1-type Rieske [2Fe-2S] center of *Thermus thermophilus*, *J. Am. Chem. Soc. 123*, 9906−9907.
5. Iwaki, M., Yakovlev, G., Hirst, J., Osyczka, A., Dutton, P. L., Marshall, D., and Rich, P. R. (2005) Direct observation of redox-linked histidine protonation changes in the iron sulfur protein of cytochrome bc_1 complex by ATR-FTIR spectroscopy, *Biochemistry 44*, 4230−4237.
6. Prince, R. C., and Dutton, P. L. (1976) Further studies on the Rieske iron−sulfur center in mitochondrial and photosynthetic systems: a p*K* on the oxidized form, *FEBS Lett. 65*, 117−119.
7. Kuila, D., and Fee, J. A. (1986) Evidence for a redox-linked ionizable group associated with the [2Fe-2S] cluster of *Thermus* Rieske protein, *J. Biol. Chem. 261*, 2768−2771.
8. Zu, Y., Couture, M. M.-J., Kolling, D. R. J., Crofts, A. R., Eltis, L. D., Fee, J. A., and Hirst, J. (2003) Reduction potentials of Rieske clusters: importance of the coupling between oxidation state and histidine protonation state, *Biochemistry 42*, 12400−12408.
9. Berry, E. A., Guergova-Kuras, M., Huang, L.-S., and Crofts, A. R. (2000) Structure and function of cytochrome *bc* complexes, *Annu. Rev. Biochem. 69*, 1005−1075.
10. Colbert, C. L., Couture, M. M.-J., Eltis, L. D., and Bolin, J. T. (2000) A cluster exposed: structure of the Rieske ferredoxin from biphenyl dioxygenase and the redox properties of Rieske FeS proteins, *Structure 8*, 1267−1278.
11. Couture, M. M.-J., Colbert, C. L., Babini, E., Rosell, F. I., Mauk, A. G., Bolin, J. T., and Eltis, L. D. (2001) Characterization of BphF, a Rieske-type ferredoxin with a low reduction potential, *Biochemistry 40*, 84−92.
12. Darrouzet, E., Valkova-Valchanova, M., and Daldal, F. (2002) The [2Fe-2S] cluster E_m as an indicator of the iron−sulfur subunit position in the ubihydroquinone oxidation site of the cytochrome bc_1 complex, *J. Biol. Chem. 277*, 3464−3470.
13. Cooley, J. W., Roberts, A. G., Bowman, M. K., Kramer, D. M., and Daldal, F. (2004) The raised midpoint potential of the [2Fe2S] cluster of cytochrome bc_1 is mediated by both the Q_O site occupants and the head domain position of the Fe−S protein subunit, *Biochemistry 43*, 2217−2227.
14. Crofts, A. R., Hong, S., Ugulava, N., Barquera, B., Gennis, R., Guergova-Kuras, M., and Berry, E. A. (1999) Pathways for proton release during ubihydroquinone oxidation by the bc_1 complex, *Proc. Natl. Acad. Sci., U.S.A. 96*, 10021−10026.
15. Hunte, C., Palsdottir, H., and Trumpower, B. L. (2003) Protonmotive pathways and mechanisms in the cytochrome bc_1 complex, *FEBS Lett. 545*, 39−46.
16. Berry, E. A., and Huang, L.-S. (2003) Observations concerning the quinol oxidation site of the cytochrome bc_1 complex, *FEBS Lett. 555*, 13−20.
17. Osyczka, A., Moser, C. C., Daldal, F., and Dutton, P. L. (2004) Reversible redox energy coupling in electron-transfer chains, *Nature 427*, 607−612.
18. Rich, P. R. (2004) The quinone chemistry of *bc* complexes, *Biochim. Biophys. Acta 1658*, 165−171.
19. Carrell, C. J., Zhang, H., Cramer, W. A., and Smith, J. L. (1997) Biological identity and diversity in photosynthesis and respiration: structure of the lumen-side domain of the chloroplast Rieske protein, *Structure 5*, 1613−1625.
20. Kauppi, B., Lee, K., Carredano, E., Parales, R. E., Gibson, D. T., Eklund, H., and Ramaswamy, S. (1998) Structure of an aromatic-ring-hydroxylating dioxygenase—naphthalene 1,2-dioxygenase, *Structure 6*, 571−586.
21. Bönisch, H., Schmidt, C. L., Schäfer, G., and Ladenstein, R. (2002) The structure of the soluble domain of an archaeal Rieske iron−sulfur protein at 1.1 Å resolution, *J. Mol. Biol. 319*, 791−805.
22. Hunsicker-Wang, L. M., Heine, A., Chen, Y., Luna, E. P., Todaro, T., Zhang, Y. M., Williams, P. A., McRee, D. E., Hirst, J., Stout, C. D., and Fee, J. A. (2003) High-resolution structure of the soluble, respiratory-type Rieske protein from *Thermus thermophilus*: analysis and comparison, *Biochemistry 42*, 7303−7317.
23. Denke, E., Merbitz-Zahradnik, T., Hatzfeld, O. M., Snyder, C. H., Link, T. A., and Trumpower, B. L. (1998) Alteration of the midpoint potential and catalytic activity of the Rieske iron−sulfur protein by changes of amino acids forming hydrogen bonds to the iron−sulfur cluster, *J. Biol. Chem. 273*, 9085−9093.
24. Schröter, T., Hatzfeld, O. M., Gemeinhardt, S., Korn, M., Friedrich, T., Ludwig, B., and Link, T. A. (1998) Mutational analysis of residues forming hydrogen bonds in the Rieske [2Fe-2S] cluster of the cytochrome bc_1 complex in *Paracoccus denitrificans*, *Eur. J. Biochem. 255*, 100−106.

25. Guergova-Kuras, M., Kuras, R., Ugulava, N., Hadad, I., and Crofts, A. R. (2000) Specific mutagenesis of the Rieske iron−sulfur protein in *Rhodobacter sphaeroides* shows that both the thermodynamic gradient and p*K* of the oxidized form determine the rate of quinol oxidation by the bc_1 complex, *Biochemistry 39*, 7436−7444.
26. Slater, E. C., and de Vries, S. (1980) Identification of the BAL-labile factor, *Nature 288*, 717−718.
27. Davidson, E., Ohnishi, T., Atta-Asafo-Adeji, E., and Daldal, F. (1992) Potential ligands to the [2Fe-2S] Rieske cluster of the cytochrome bc_1 complex of *Rhodobacter capsulatus* probed by site-directed mutagenesis, *Biochemistry 31*, 3342−3351.
28. van Doren, S. R., Gennis, R. B., Barquera, B., and Crofts, A. R. (1993) Site-directed mutations of conserved residues of the Rieske iron−sulfur subunit of the cytochrome bc_1 complex of *Rhodobacter sphaeroides* blocking or impairing quinol oxidation, *Biochemistry 32*, 8083−8091.
29. Merbitz-Zahradnik, T., Zwicker, K., Nett, J. H., Link, T. A., and Trumpower, B. L. (2003) Elimination of the disulfide bridge in the Rieske iron−sulfur protein allows assembly of the [2Fe-2S] cluster into the Rieske protein but damages the ubiquinol oxidation site in the cytochrome bc_1 complex, *Biochemistry 42*, 13637−13645.
30. Zu, Y., Fee, J. A., and Hirst, J. (2002) Breaking and re-forming the disulfide bond at the high-potential, respiratory-type [2Fe-2S] center of *Thermus thermophilus*: characterization of the sulfhydryl state by protein-film voltammetry, *Biochemistry 41*, 14054−14065.
31. Liebl, U., Sled, V., Brasseur, G., Ohnishi, T., and Daldal, F. (1997) Conserved nonliganding residues of the *Rhodobacter capsulatus* Rieske iron−sulfur protein of the bc_1 complex are essential for protein structure, properties of the [2Fe-2S] cluster, and communication with the quinone pool, *Biochemistry 36*, 11675−11684.
32. Brasseur, G., Sled, V., Liebl, U., Ohnishi, T., and Daldal, F. (1997) The amino-terminal portion of the Rieske iron−sulfur protein contributes to the ubihydroquinone oxidation site catalysis of the *Rhodobacter capsulatus* bc_1 complex, *Biochemistry 36*, 11685−11696.
33. Klingen, A. R., and Ullmann, G. M. (2004) Negatively charged residues and hydrogen bonds tune the ligand histidine pK_a values of Rieske iron−sulfur proteins, *Biochemistry 43*, 12383−12389.
34. Zhang, Z. L., Huang, L. S., Shulmeister, V. M., Chi, Y.-I., Kim, K. K., Hung, L.-W., Crofts, A. R., Berry, E. A., and Kim, S.-H. (1998) Electron transfer by domain movement in cytochrome bc_1, *Nature 392*, 677−684.
35. Link, T. A., Hagen, W. R., Pierik, A. J., Assmann, C., and von Jagow, G. (1992) Determination of the redox properties of the Rieske [2Fe-2S] cluster of bovine heart bc_1 complex by direct electrochemistry of a water-soluble fragment, *Eur. J. Biochem. 208*, 685−691.
36. Link, T. A., Saynovits, M., Assmann, C., Iwata, S., Ohnishi, T., and von Jagow, G. (1996) Isolation, characterization and crystallization of a water-soluble fragment of the Rieske iron−sulfur protein of bovine-heart mitochondrial bc_1 complex, *Eur. J. Biochem. 237*, 71−75.
37. Doeg, K. A., and Ziegler, D. M. (1962) Simplified methods for the estimation of iron in mitochondria and submitochondrial fractions, *Arch. Biochem. Biophys. 97*, 37−40.
38. Nakamura, M., Saeki, K., and Takahashi, Y. (1999) Hyperproduction of recombinant ferredoxins in *Escherichia coli* by coexpression of the ORF1-ORF2-*iscS-iscU-iscA-hscB-hscA-fdx*-ORF3 gene cluster, *J. Biochem. 126*, 10−18.
39. Zu, Y., Di Bernardo, S., Yagi, T., and Hirst, J. (2002) Redox properties of the [2Fe-2S] center in the 24 kDa (NQO2) subunit of NADH: ubiquinone oxidoreductase (complex I), *Biochemistry 41*, 10056−10069.
40. Agarwal, A., Li, D., and Cowan, J. A. (1995) Role of aromatic residues in stabilization of the [Fe_4S_4] cluster in high-potential iron proteins (HiPIPs): physical characterization and stability studies of Tyr-19 mutants of *Chromatium vinosum* HiPIP, *Proc. Natl. Acad. Sci., U.S.A. 92*, 9440−9444.

BI050189X